Nonlinear optical generation from noble metals and aluminum films in various geometric configurations

Chin-Ching Tzeng and Juh Tzeng Lue
Department of Physics, National Tsing-Hua University, 855 Kuang Fu Road, Hsin-Chu, Taiwan 30043, Republic of China
(Received 19 January 1988; revised manuscript received 2 May 1988)

Based on the hydrodynamic theory of an electron gas, we have calculated the second-harmonic generation (SHG) from metal surfaces in various geometric configurations. The SHG of single-boundary surface plasmons coupled using the Kretschmann geometry is ten times larger for gold, copper, and silver, and 100 times larger for aluminum films than the SHG from the bare metal reflectors. The SHG due to long-range surface plasmons in a modified Kretschmann geometry with a very thin metal film sandwiched between two dielectric layers is typically over two orders of magnitude larger than that from the simple Kretschmann geometry. Enhanced SHG is presumed as the thickness of the index-matched liquid layer and the metal films are suitably adjusted because of the resonant interference.

I. INTRODUCTION

The first theoretical prediction of the second-harmonic generation (SHG) of light from a free-electron gas was presented by Jha[1] in 1965. Later, the first conclusive experimental observation of the SHG from a silver film excited by a ruby laser light was reported by Brown *et al.*[2,3] Recently, research in SHG from metal surfaces has been expedited by discoveries of the enhanced scattered SHG from roughened silver surfaces,[4] from molecular monolayers adsorbed on a silver surface,[5,6] and from nonlinear surface-plasmon effects.[7–9] Exploiting SHG from the surface of centrosymmetric media as a new probe for studies of surface physics has been recently demonstrated by several authors.[10]

An excellent review discussing SHG from metal surfaces was published by Sipe and Stegeman.[11] The sources of SHG on a metal surface consist of a "volume" current density which extends over skin depth and a "surface" current density penetrating only a few Fermi wavelengths into the metal (the so-called selvedge region). The free-electron model is inadequate to describe the electron dynamics in the selvedge region. Rudnick and Stern[12] first pointed out the limitations of the free-electron model in describing the SHG surface-current sources and proposed two phenomenological parameters a and b to estimate the size of these current sources. Sipe *et al.*[13] have given an explicit expression for these parameters with a free-electron hydrodynamic model and have introduced an effective plasma frequency. They have done calculations with $b=-1$ for a smooth metal surface, allowing the parameter a to be determined by experiments. This theory along with the experimental results for the SHG in a total-internal-reflection (TIR) geometry from a prism-metal interface over a broad range of incident angles can successfully determine the parameter a of noble metals and aluminum films.[14,15]

Recently developed theories[16] on the properties of coupled surface-plasmon modes formed on two surfaces of a thin metal film bounded by index-matched dielectrics have stimulated both theoretical and experimental interest in nonlinear optics.[8,9,17,18] The two modes can be treated as antisymmetric and symmetric (in transverse magnetic field distribution) coupled modes of the single-boundary surface plasmons (SBSP's) on the two metal surfaces. The former is described as the long-range surface-plasmon (LRSP) mode and the latter as the short-range surface-plasmon (SRSP) mode. A demonstration of resonant SHG from quartz crystal, owing to phase-matched and -unmatched excitation of the fundamental LRSP and SRSP modes with the harmonic LRSP mode, has been reported.[8,9]

In this work, we first derive the formulas for evaluating the SHG of metal films under a modified Kretschmann geometry on the basis of electron-gas hydrodynamic theory. We assume that the boundary media of the metal film have negligible nonlinear susceptibilities and that the second-harmonic (SH) waves are essentially generated from the bulk and selvedge regions of the film. Numerical calculations show that SHG from thin metal films with LRSP excitation is largely enhanced in comparison with that from an attenuated-total-reflection (ATR) geometry. We find silver metal films to be the most efficient substrates for coupling surface plasmons. An anomalously large nonlinear reflectance is found at some specific incident angles for thick films with an extremely narrow angular width. This resonance peak is assumed to be due to the interference of the multiple reflection of the SH wave within the multiple boundaries and the sensitive angular dependence on the excitation of LRSP.

II. THEORY

When a p-polarized wave is incident upon a metal film of thickness d_3 in the Sarid configuration, a free transverse-mode (TM) wave can be excited in the thin metal layer satisfying the dispersion relation given by[16,19]

$$w_3 d_3 = \tan^{-1}(\beta_{32}) + \tan^{-1}(\beta_{34}) + m\pi \ , \quad (1)$$

where

$$\beta_{ij} \equiv \frac{\epsilon_i(\mathbf{k}_{sp}^2 - \tilde{\omega}_j^2)^{1/2}}{\epsilon_j(\tilde{\omega}_i^2 - \mathbf{k}_{sp}^2)^{1/2}} , \tag{2}$$

m is the mode number (a positive integer), $\tilde{\omega}_i = (\omega/c)\sqrt{\epsilon_i(\omega)}$ is the wave vector in ith medium with dielectric constant $\epsilon_i(\omega)$, and $\mathbf{k}_{sp} = k'_{sp} + ik''_{sp}$ is the propagation wave vector of the guided surface-plasmon mode (with prime and double prime indicating the real and imaginary parts, respectively). Equation (1) can elucidate the wave vector $\mathbf{k}_{sp}$ for LRSP and SRSP modes in terms of the metal film thickness d_3.

The hydrodynamic theory[13] is exploited to describe the nonlinear response of electrons (including free and bound electrons) in the metal. Considering a fundamental wave with angular frequency ω impinging on a metal film with the geometry as shown in Fig. 1, the second-harmonic polarization generated in the bulk region of metal is

$$\mathbf{P}_{NL}^{B}(\mathbf{r}) = -\frac{q}{2m_e\omega^2}\left[\frac{\epsilon_m(2\omega)-1}{2\pi}\right]\nabla\mathbf{E}_m(\mathbf{r})\cdot\mathbf{E}_m(\mathbf{r}) . \tag{3}$$

This causes an effective nonlinear current density at the selvedge region of metal as given by

$$\mathbf{J}_{NL}^{S}(\mathbf{r}) = -2\omega i\mathbf{Q}e^{i\mathbf{K}\cdot\mathbf{r}}\delta(z - z_0^{(\pm)}) , \tag{4}$$

where $i = \sqrt{-1}$, the interface is at $z = z_0$, and the parallel and normal components of the dipole moment per unit area $\mathbf{Q}$ are expressed by

$$Q^k = (\mp)\frac{qb}{2m_e\omega^2}\left[\frac{\epsilon_m(\omega)-1}{4\pi}\right]E_m^k(z_0^{(\mp)}E_m^k z_0^{(\mp)}) ,$$

and

$$Q^z = (\mp)\frac{qa}{4m_e\omega^2}\left[\frac{\epsilon_m(\omega)-1}{4\pi}\right][E_m^z(z_0^{(\mp)})]^2 , \tag{5}$$

respectively. Here $\epsilon_m(\omega)$ and $\epsilon_m(2\omega)$ are the dielectric constants of the metal at fundamental and harmonic frequencies, respectively, E_m^k and E_m^z are the tangential and normal components of the fundamental electric field inside the metal, q is the charge of electron, m_e is the mass of electron, and a and b are the phenomenological parameters. The plus and minus signs as shown in Eq. (5) are used to indicate the current sheet located outside the "bulk metal," specifying upward and downward along the z axis, respectively.

The three geometrical configurations usually applied to the study of surface waves are the external reflection (ER), attenuated total reflection (ATR or Kretschmann), and modified Kretschmann (or Sarid) geometries, as shown in Figs. 1(a), 1(b), 1(c), respectively. The electric field in each medium can be calculated by the transfer-matrix method.[19] Once the electric field in the metal film is calculated, the induced nonlinear polarization can be specified by Eqs. (3) and (4). The generated second-harmonic fields can be derived either by a straightforward application of Maxwell's equations or by a simple extension of the transfer-matrix theory.[13] The second-harmonic reflection coefficient R is defined to be the ratio of the reflected SHG irradiance to the square of the incident fundamental irradiance, while the field enhancement factor is defined to be the ratio of the absolute square of the electric field at the surface just outside the metal film to that of the incident wave inside the prism. We can explicitly derive the value of R in each of the three geometries for a p-polarized incident beam as the following.

(i) For the ER geometry,

$$R_{ER} = \frac{8\pi q^2}{m_e^2 c^3 \omega^2}\sin^2\theta\cos^4\theta\frac{|\epsilon_m(\omega)|^2|\epsilon_m(\omega)-1|^2\left|\frac{\epsilon_m(2\omega)}{\epsilon_m(\omega)}a\sin^2\theta - \frac{2b}{\epsilon_m(\omega)}G_1G_2 + \frac{1}{2}\right|^2}{|\epsilon_m(\omega)\cos\theta + G_1|^4|\epsilon_m(2\omega)\cos\theta + G_2|^2} , \tag{6}$$

where θ is the incident angle,

$$G_1 \equiv [\epsilon_m(\omega) - \sin^2\theta]^{1/2} ,$$

and

$$G_2 \equiv [\epsilon_m(2\omega) - \sin^2\theta]^{1/2} . \tag{7}$$

(ii) For the Kretschmann geometry,

$$R = \frac{2\pi}{c}\frac{N_1}{n_1^2}|A|^2 T , \tag{8}$$

where n_1 and N_1 are the refractive indices of the prism at ω and 2ω, and A is the ratio of the second-harmonic electric field to the square of the fundamental field inside the prism and is denoted by $A = A_m + A_0 + A_d$. The three terms are the SHG contributing from the bulk metal, front prism-metal selvedge, and back metal-glass substrate, respectively. The factor T contains the Fresnel and geometrical factors describing the coupling of the fundamental waves from air into the prism and the exiting of the second-harmonic wave from the prism backward into the air. The explicit expressions for T, A_m, A_0, and A_d of this geometry have been prescribed by the present authors.[15]

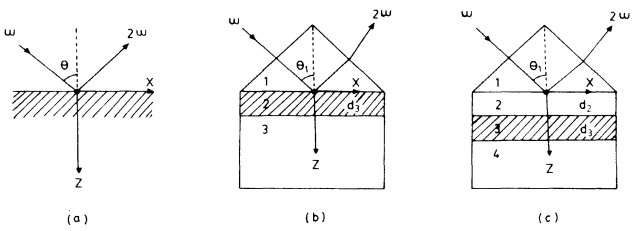

FIG. 1. Three configurations for SHG: (a) the external reflection (ER), (b) the Kretschmann, and (c) modified Kretschmann (or Sarid) geometries.

The electric field enhancement factor η with SBSP at the metal-glass substrate selvedge is derived as

$$\eta \equiv \left| \frac{m_{123} t_{12} e^{iw_2 d_3}}{\tilde{\omega}_2} \right|^2 [|k(1+r_{23})|^2 + |w_2(1-r_{23})|^2] , \tag{9}$$

where d_3 is the thickness of metal film, $w_i = (\tilde{\omega}_i^2 - \mathbf{k}^2)^{1/2}$ is the normal component of the wave vector in the ith medium, $\mathbf{k}$ is the tangential component of the free-space wave vector ω/c, m_{123} is the modification factor due to multiple reflection at ω, and t_{ij} and r_{ij} are the Fresnel coefficients for transmission and reflection of p-polarized wave, respectively, and given by

$$t_{ij} = \frac{2(\epsilon_i \epsilon_j)^{1/2} w_i}{w_i \epsilon_j + w_j \epsilon_i} \tag{10a}$$

and

$$r_{ij} = \frac{w_i \epsilon_j - w_j \epsilon_i}{w_i \epsilon_j + w_j \epsilon_i} . \tag{10b}$$

(iii) For the modified Kretschmann (or Sarid) geometry, the expression of second-harmonic coefficient R in the Sarid geometry is the same as Eq. (8), except that the A_m, A_0, and A_d represent the SHG from the bulk metal, the liquid-layer–metal-selvedge, and the metal-glass substrate interfaces, respectively. They can be derived as

$$\begin{aligned} A_m \equiv & M_{1234} T_{321} (m_{1234} m_{234} t_{12} t_{23} e^{iw_2 d_2})^2 \frac{K(q/m_e)[\epsilon_3(2\omega)-1]}{ic^2 W_3 \tilde{\Omega}_3 \tilde{\omega}_3^2} \\ & \times \{(1+R_{34}) e^{i(2w_3 d_3 + W_3 d_3)} [k^2(1+r_{34})^2 + w_3^2(1-r_{34})^2] \\ & - (1+R_{34} e^{2iW_3 d_3})[k^2(1+r_{34} e^{2iW_3 d_3})^2 + w_3^2(1-r_{34} e^{2iw_3 d_3})^2]\} , \end{aligned} \tag{11}$$

$$A_0 \equiv 2\pi i M_{1234} T_{321} \left[\frac{K\tilde{\Omega}_3}{W_3} (1+R_{34} e^{2iW_3 d_3}) Q_0^z + \frac{\tilde{\Omega}_2}{\tilde{\Omega}_3} (1-R_{34} e^{2iW_3 d_3}) Q_0^k \right] , \tag{12}$$

and

$$A_d \equiv 2\pi i M_{1234} T_{321} T_{43} e^{iW_3 d_3} \left[\frac{K\tilde{\Omega}_4}{W_4} Q_d^z + \frac{\tilde{\Omega}^2}{\tilde{\Omega}_4} Q_d^k \right] , \tag{13}$$

respectively, where

$$m_{1234} = (1 + r_{12} r_{234} e^{2iw_2 d_2})^{-1}$$

and

$$M_{1234} = (1 + R_{12} R_{234} e^{2iW_2 d_2})^{-1} \tag{14}$$

are the modification factors due to reflections between multiple interfaces at ω and 2ω. The factor T_{321} in the equations above represents the transmission from the third layer to the first layer at 2ω, and r_{234} is the reflection factor due to second, third, and fourth layers at ω. They are written as

$$T_{321} = M_{321} T_{32} T_{21} e^{iW_2 d_2}$$

and

$$r_{234} = m_{234}(r_{23} + r_{34} e^{2iw_3 d_3}) , \tag{15}$$

respectively, where

$$m_{ijk} = (1 + r_{ij} r_{jk} e^{2iw_j d_j})^{-1} . \tag{16}$$

We use the capital letters to indicate the corresponding quantities evaluated at $\Omega = 2\omega$ and $K = 2k$. The subscripts 1, 2 , 3, and 4 denote the prism, the index-matched liquid layer with thickness d_2, the metal with thickness d_3, and the glass substrate, respectively. Here Q is the dipole moment per unit area of the second-harmonic current sheets. The tangential and normal components for the liquid-layer–metal-selvedge are

$$Q_0^k = bFkw_3(r_{34} e^{4iw_3 d_3} - 1)$$

and

$$Q_0^z = aF \frac{k^2}{2} (r_{34} e^{2iw_3 d_3} + 1)^2 , \tag{17}$$

respectively, while at the metal–glass-substrate selvedge, the components are

$$Q_d^k = -bFkw_3(r_{34}^2 - 1) e^{2iw_3 d_3} ,$$

and

$$Q_d^z = -aF \frac{k^2}{2} (r_{34} + 1)^2 e^{2iw_3 d_3} , \tag{18}$$

where the common factor F is

$$F = \frac{q}{m_e} \frac{[\epsilon_3(\omega) - 1]}{8\pi\omega^2 \tilde{\omega}_3^2} (m_{1234} m_{234} t_{12} t_{23} e^{iw_2 d_2})^2 , \tag{19}$$

in which the $\epsilon_3(\omega)$ is the metal dielectric constant at fundamental frequency.

The electric field enhancement factors at liquid-layer–metal selvedge and metal–glass-substrate selvedge are denoted by η_{23} and η_{34}, respectively. According to the transfer-matrix method, the explicit formulas for η_{23} and η_{34} are derived as

TABLE I. Parameters for theoretical calculations.

Metal	ϵ_{ω} (1.06 μm)	$\epsilon_{2\omega}$ (0.53 μm)	a	Ref.
Au	$-48.24+i3.58$	$-4.53+i2.46$	-1.4	15,20
Ag	$-67.03+i2.44$	$-11.9+i0.33$	0.9	14,20
Cu	$-49.13+i4.91$	$-5.48+i5.86$	-1.6	15,20
Al	$-95+i33$	$-33+i10$	1.5	14,20

Prism	Index of refraction 1.06 μm	0.53 μm	
Schott BK-7 glass	1.507	1.520	22
Schott SF-59 glass	1.908	1.970	22
Glass-substrate	1.4497	1.4608	23

$$\eta_{23}=\left|\frac{m_{1234}m_{234}t_{12}t_{23}e^{iw_2d_2}}{\tilde{\omega}_3}\right|^2 \times[|k(1+r_{34}e^{2iw_3d_3})|^2+|w_3(1-r_{34}e^{2iw_3d_3})|^2] \quad (20)$$

and

$$\eta_{34}=\left|\frac{m_{1234}m_{234}t_{12}t_{23}e^{i(w_2d_2+w_3d_3)}}{\tilde{\omega}_3}\right|^2 \times[|k(1+r_{34})|^2+|w_3(1-r_{34})|^2] , \quad (21)$$

respectively.

III. THEORETICAL RESULTS AND CONCLUSIONS

The optical constants and phenomenological parameter a exploited in this theoretical calculation are shown in Table I. The prisms used for coupling the surface plasmons into the films are made of Schott SF-59 glass.

Figure 2 shows the second-harmonic generation in the Kretschmann geometry versus the internal incident angles. The coupling prism is a Schott BK-7 glass prism for the total-internal-reflection experiments,[14,15,21] and the film thickness is 3000 Å. The maximum values of second-harmonic intensities for silver, gold, copper, and aluminum opaque films are 16.6×10^{-20}, 6.14×10^{-20},

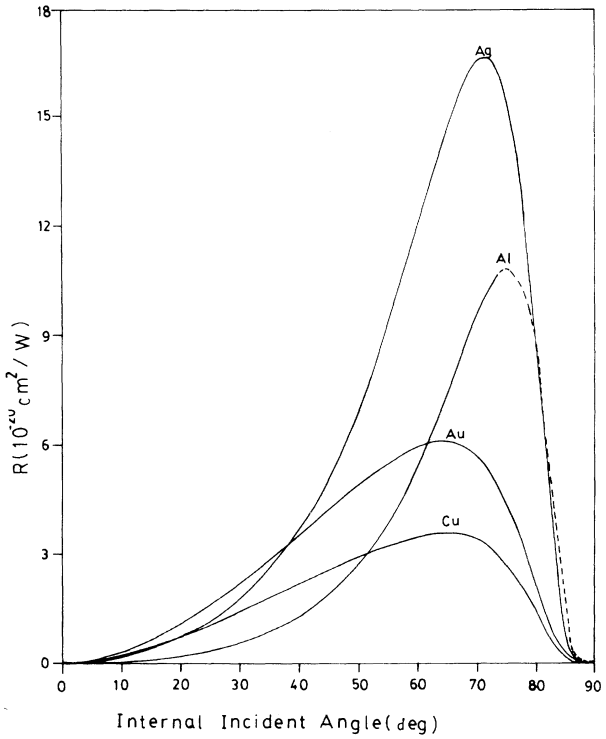

FIG. 2. Second-harmonic reflection coefficient R by TIR geometry vs the internal incident angle θ_1 for silver, gold, copper, and aluminum films, respectively.

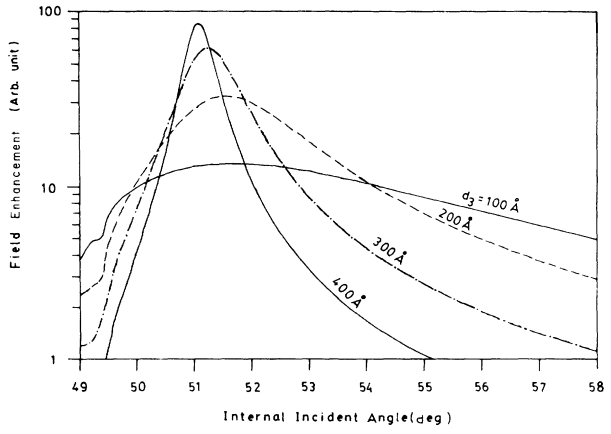

FIG. 3. Field enhancement of SBSP in Kretschmann geometry for gold-metal film as a function of the internal incident angle at several covering silver-film thicknesses.

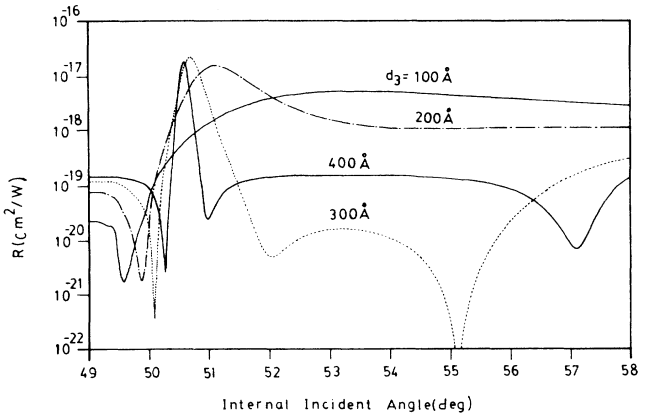

FIG. 4. Second-harmonic reflection coefficient as a function of the internal incident angle in Kretschmann geometry at four silver-film thicknesses.

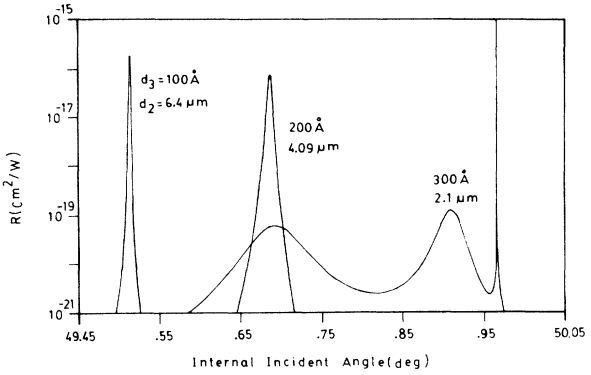

FIG. 6. Second-harmonic reflection coefficient as a function of the internal incident angle in Sarid geometry with LRSP excitation at sets of gold-film and index-matched liquid-layer thicknesses.

3.61×10^{-20}, and 10.9×10^{-20} cm^2/W, with the corresponding incident angles of 72°, 64°, 65°, and 75°, respectively. A comparison between the second-harmonic intensity from the TIR geometry and that from the ER geometry indicates that the SHG from the total internal reflection critically depends on the value of the phenomenological parameter a.

Figure 3 shows the electric field enhancement factors η in the Kretschmann geometry as functions of internal incident angle θ, at various gold-film thicknesses for the fundamental wave at $\lambda=1.06$ μm. As the film thicknesses becomes thinner, the excitation intensities of surface waves on both sides of the metal become equivalent. The coupling of these two waves will smear out the attenuated-total-reflection peak, as occurring in a thick film, and the acceptance angle broadens.

Figures 4 and 5 show the second-harmonic reflection coefficients R of silver and gold, respectively, with surface plasmons in Kretschmann geometry versus internal incident angle at several film thicknesses. The interference structures in the wings of the surface-plasmon resonance at a certain film thickness are observed for all of these metals. The silver film is found to show the largest coupling of surface plasmons.

Figures 6, 7, and 8 show the nonlinear reflection coefficients R for silver, gold, and aluminum thin films with fundamental LRSP excitation at $\lambda=1.06$ μm, as functions of internal incident angle in the Sarid geometry. For $d_3=100$ Å the second-harmonic generation with LRSP excitation is over two orders of magnitude, and larger than that from the SBSP excitation. An unusual sharp peak occurs near the vicinity of $\theta_1=49.9658°$, indicating that a SHG of R is over five orders of magnitude larger than those from the LRSP mode. This angle corresponds to the incident angle for obtaining a maximum value of $|M_{1234}|^2$ and is presumed to be due to resonance interference of the second-harmonic waves reflecting between several boundaries, and is due to the critical sharp

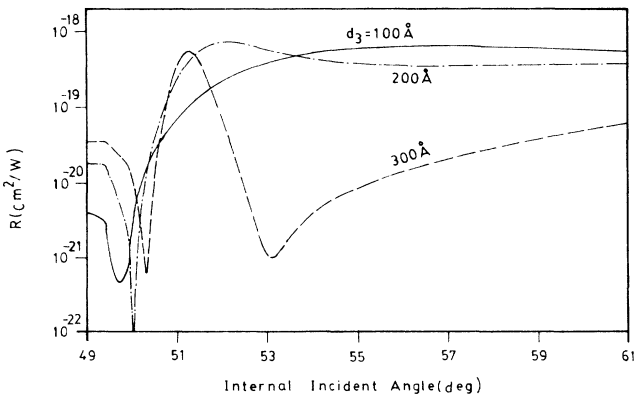

FIG. 5. Second-harmonic reflection coefficient as a function of the internal incident angle in Kretschmann geometry at three gold-film thicknesses.

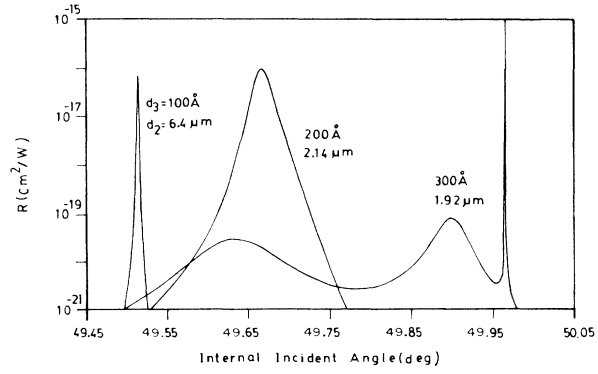

FIG. 7. Second-harmonic reflection coefficient as a function of the internal incident angle in Sarid geometry with LRSP excitation at sets of copper-film and index-matched liquid-layer thicknesses.

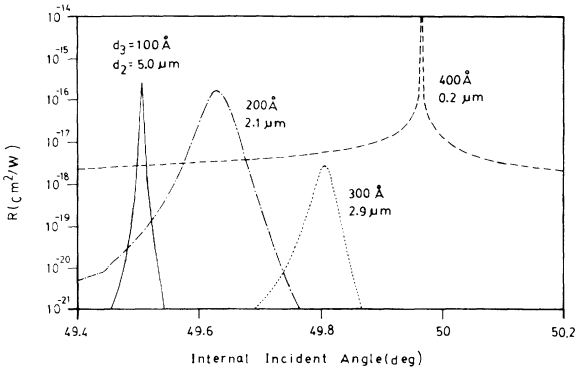

FIG. 8. Second-harmonic reflection coefficient as a function of the internal incident angle in Sarid geometry with LRSP excitation at sets of aluminum-film and index-matched liquid-layer thicknesses.

angle for excitation of LRSP at thick films. It is difficult to observe this phenomenon experimentally, since the angular width of this resonance peak is much narrower than the divergent angle of presently available laser beams.

In summary, we have explicitly expressed the formulas of SHG from metals in ER, ATR, and Sarid geometries. We have also derived the expressions of electric field enhancement factors in Kretschmann and Sarid geometries. The field enhancement factor of fundamental LRSP with very thin metal films is typically one order of magnitude larger than that of SBSP. The second-harmonic intensities resulting from coupling of SBSP's are, respectively, one order of magnitude for gold and copper films, and for silver and aluminum two orders of magnitude larger than those from external reflection. The second-harmonic generation with LRSP excitation of thin metal films is over two orders of magnitude larger than that of SBSP. The SHG's from all metal films in Sarid geometry are enhanced over five orders of magnitude at one particular angle of incidence when the thickness of the index-matched liquid layer and the metal film are properly adjusted. Silver films in various geometries are found to be the most efficient SHG materials. The second-harmonic reflection coefficients are very sensitive to the value of the phenomenological parameter a in Kretschmann and Sarid geometries.

Since the lifetime of the surface plasma wave greatly depends on the properties of metal surface, the surface nonlinear-wave generation can be exploited as a sensitive probe for characterizing surface conditions such as roughness and contamination. Deck and Grygier,[24] using a Green's-function technique, concluded that a rough metal surface can enhance the coupling of the incident wave in a surface-plasmon mode and interferes with the fundamental field to produce a second-harmonic wave which radiates from the metal in a narrowly defined direction. However, a rough metal surface implies an increased surface scattering of electrons, which greatly reduces the propagation decay time of the LRSP, resulting in a degrading of the second-harmonic generation efficiency. Radiation damping[25] accounts for the radiative losses of the oscillating electric dipole of the metal particles. It can affect the depolarization factor with a correction term proportional to the particle volume and inversely proportional to λ^3. Therefore, the radiation damping is not severe in this smooth, long-wavelength system.

ACKNOWLEDGMENTS

This work is supported by the National Science Council of the Republic of China and the Materials Science Center of National Tsing Hua University.

[1]S. J. Jha, Phys. Rev. **140**, A2020 (1965).
[2]F. Brown, R. E. Parks, and A. M. Sleeper, Phys. Rev. Lett. **14**, 1029 (1965).
[3]F. Brown and R. E. Parks, Phys. Rev. Lett. **16**, 507 (1966).
[4]C. K. Chen, A. R. B. Decastro, and Y. R. Shen, Phys. Rev. Lett. **46**, 145 (1981).
[5]C. K. Chen, T. F. Heinz, D. Ricard, and Y. R. Shen, Phys. Rev. Lett. **46**, 1010 (1981).
[6]G. T. Boyd and Y. R. Shen, Opt. Lett. **11**, 97 (1986).
[7]H. J. Simon, D. E. Mitchell, and J. G. Watson, Phys. Rev. Lett. **33**, 1531 (1974).
[8]J. C. Quail, J. G. Rako, H. J. Simon, and R. T. Deck, Phys. Rev. Lett. **50**, 1987 (1983).
[9]J. C. Quail and H. J. Simon, J. Appl. Phys. **56**, 2589 (1984).
[10]H. W. K. Tom, C. M. Mate, X. D. Zhu, J. E. Crowell, T. F. Heinz, G. A. Somorjai, and Y. R. Shen, Phys. Rev. Lett. **52**, 348 (1984).
[11]J. E. Sipe and G. I. Stegeman, in *Surface Polaritons: Electromagnetic Waves at Surfaces and Interfaces*, edited by V. M. Agranovish and D. L. Mills (North-Holland, Amsterdam, 1982), p. 661.
[12]J. Rudnick and E. A. Stern, Phys. Rev. B **4**, 4274 (1971).
[13]J. E. Sipe, V. C. Y. So, M. Fukui, and G. I. Stegeman, Phys. Rev. B **21**, 4389 (1980).
[14]J. C. Quail and H. J. Simon, Phys. Rev. B **31**, 4900 (1985).
[15]C. C. Tzeng and J. T. Lue, Surf. Sci. **192**, 491 (1987).
[16]D. Sarid, Phys. Rev. Lett. **47**, 1927 (1981).
[17]G. I. Stegeman and J. J. Buke, Appl. Phys. Lett. **41**, 906 (1982).
[18]R. T. Deck and D. Sarid, J. Opt. Soc. Am. **72**, 1613 (1982).
[19]J. E. Sipe, Surf. Sci. **84**, 75 (1979).
[20]P. B. Johnson and R. W. Christy, Phys. Rev. B **6**, 4370 (1972).
[21]*American Institute of Physics Handbook*, edited by D. E. Gray (McGraw-Hill, New York, 1972).
[22]Optical Glass Inc. Catalog No. 18642 (unpublished).
[23]*Handbook of Optical Constants of Solids*, edited by Edward D. Palik (Academic, New York, 1985), p. 760.
[24]R. T. Deck and R. F. K. Grygier, Appl. Opt. **23**, 3202 (1984).
[25]A. Wokaun, Solid State Phys. **38**, 223 (1984).